GSI-95-08
REPORT
JULY 1995
ISSN 0171-4546

LARGE SIZE FOIL - MICROCHANNEL-PLATE TIMING DETECTORS

S. SARO, R. JANIK, S. HOFMANN, H. FOLGER,
F.P. HESSBERGER, V. NINOV. H.J. SCHÖTT,
A.N. ANDREYEV, A.P. KABACHENKO, A.V. YEREMIN

CERN LIBRARIES, GENEVA
SCAN-9507262
SW 9531

Gesellschaft für Schwerionenforschung mbH
Postfach 110552 · D-64220 Darmstadt · Germany

Large Size Foil - Microchannel-Plate Timing Detectors

Š. Šaro, R.Janik

Comenius University Bratislava, Slovakia

S.Hofmann, H.Folger, F.P.Heßberger, V.Ninov, H.J.Schött

Gesellschaft für Schwerionenforschung, Darmstadt, Germany

A.N.Andreyev, A.P.Kabachenko, A.V.Yeremin

Laboratory of Nuclear Reactions, JINR Dubna, Russia

Abstract

To measure the velocity of slow heavy nuclei, created as evaporation residues in nuclear reactions, large area thin timing detectors should be used. An overwiev is given on principial properties and possibilities of foil - micro-channel plate timing detector units and the properties of many time-of-flight (TOF) systems of this type are analysed. Two new large area foil - micro-channel plate TOF systems are presented: the TOF unit at the velocity separator SHIP, GSI Darmstadt ($\approx$ 55 cm^2 active area, $\geq$ 99% detection efficiency, 100% transparency and $\leq$ 700 ps time resolution) and the TOF system of the electrostatic separator VASSILISSA, JINR Dubna ($\approx$ 50 cm^2 active area, 99.99% detection efficiency, 90% transparency and $\approx$ 500 ps time resolution). Both systems are uniqe in size and conditions of their exploitation.

1. Introduction

The detectors, described in this work, are based on the registration of secondary electrons (SEs), produced by ionising particles passing a thin foil (emitter foil). The low energy SEs, emerging from the foil, are accelerated by an electric field and deflected by an electric or magnetic field to the surface of a micro-channel electron multiplier plate (MCP). The timing pulse is derived from the anode of the MCP detector unit. Instead of a single anode plate a multi-strip anode can be used which enables to determine the position of the electron avalanche through the MCP and in the case of isochronous SE trajectories also to determine the trajectory of the detected ions. As a rule, the emitter foil is mounted perpendicular to the direction of the detected ions. Secondary electrons are emitted from both sides of the foil. From the point on the foil, where the ion penetrated, not only electrons are emitted, but also X-rays.

There are several possibilities how to accelerate the SEs and how to direct them to the MCP surface, but there are, in principle, two basic systems which are extensively used.

1.1. TOF detectors using crossed electric and magnetic fields.

The schematic drawing of this type of a foil - MCP detector is shown in Fig.1. The accelerating electric field E is created in between two electrodes, a few cm apart each other. The applied magnetic field B is oriented perpendicular to the plane of the drawing. The secondary electron trajectories are isochronous cycloids, reflecting on the MCP the point, where the ion penetrated the foil. The trajectory of an electron in perpendicular electric and magnetic fields is cycloidal. For 2π geometry the parameters of the trajectory can be expressed in accordance with Fig.1. as

$$l = \frac{2\pi mE}{eB^2} = 3.572 \times 10^{-7} E/B^2, (cm) \tag{1}$$

$$h = \frac{2me}{eB^2} = 1.137 \times 10^{-7} E/B^2 = l/\pi, (cm) \tag{2}$$

$$t = \frac{2\pi m}{eB} = 0.03572/B, (ns) \tag{3}$$

where l - is the lateral displacement in cm, h - amplitude of the cycloid in cm, t - transition time of SEs in ns, E - electrostatic field in V/cm, B - magnetic field in Tesla, m - electron mass, e- electron charge. Details are given in refs. (BO1, ZE1).

In another variant of this type of foil-MCP detector the SEs, emitted from the foil are accelerated with a grid, apart from the foil only a few mm. Passing the grid the SEs are moving with a constant velocity v in a homogeneous magnetic field B. In this case the circular motion of the SEs is expressed by the known condition

$$\frac{mv^2}{r} = evB \tag{4}$$

or

$$r = \frac{mv}{eB} = \frac{\sqrt{2mE}}{eB}, \tag{5}$$

where r is the radius of the electron trajectory, E is the kinetic energy given to the SEs by the accelerating grid. The other quantities are denoted as before. Replacing the constants by numerical values we have

$$r = 8.42 \times 10^3 \sqrt{E}/B \tag{6}$$

where E is in Joule, B in Tesla and r in meters.
Time t for one turn of an accelerated electron is equal to

$$t = 2\pi r/v = \pi r\sqrt{2m/E} = 0.0356/B, (ns) \tag{7}$$

For a quarter-turn and for a half-turn system

$$t_{90^o} = 0.0089/B, (ns); t_{180^o} = 0.0178/B, (ns) \quad (8)$$

In the case of the quarter-turn type detector the accelerated SEs do not have equally long trajectories and consequently they will have different transition times as it shown in Fig.2. The second disadvantages is the presence of wire grids in the trajectory of the detected ions.

1.2. Electrostatic TOF detectors.

The second basic type of a foil-MCP detector is based on an electrostatic mirror (Fig.3) with 90^o bending. The SEs emitted from the foil are accelerated by a grid G1 to the energy of about 2 keV and deflected by 90^o by an electrostatic mirror, formed by grids G2 and G3, onto the channel plate MCP1. The acceleration grid G1, the inner mirror grid G2 and the MCP1 upper surface have the same potential. The outer mirror grid G3 has a higher negative potential as grid G2 by 350 - 400 Volts. The trajectories of the SEs are isochronous. Electrostatic mirror type foil-MCP detectors are described in details by several authors (BU1, DE1, HE1, HE2). The construction of this type of detectors is relatively simple, their disadvantage is the presence of three layers of wires in the projectiles trajectory (six layers of wires for collecting SEs in both, backward and forward directions and twelve layers of wires in the case of such a TOF system).

2. Foils and Secondary Electrons

The secondary electron emission (SEE) is a prompt surface effect. Only a very thin surface layer of a target foil material is involved into the process. The SEE yield and the obtained output signal are proportional to the energy loss dE/dx of the incident ion. According to the measurements made by C.C. Dedman et al. (DE2) with light ions, the SEE yield is smaller in backward direction with respect to the ions trajectory. At ion velocities about 3×10^8 cm/s the ratio of backward emitted SEs γ_b to the total SEE yield γ is $\beta = \gamma_b/\gamma \approx 0.4$. At ion velocities about 5×10^8 cm/s $\beta \approx 0.35$ and at ion velocities about 7×10^8 cm/s $\beta \approx 0.32$.

There are considerably large differences in the shape of secondary electron energy spectra, induced by light ions and heavy ions. The number of emitted SEs is a quantitative function of the projectile's nuclear charge. The heavier projectile produces comparatively more SEs of higher energy in both, forward and backward hemispheres (PF3). The SEs emitted into the backward hemisphere have a relatively small high energy component compared to the forward hemisphere (see Tab.1 and Tab.2.). Therefore the collection of SEs in the backward direction can give better time resolution at lower pulse height and on the contrary the collection of SEs in the forward direction can give higher pulse height but the time resolution may slightly decrease. The average energy of the emitted SEs given in ref. (PF3) is relatively high and the most energetic SEs may have more than 3 keV maximum energy (PF2,PF3).

No high energy SEs are reported by H.J. Frischkorn et al. (FR1), SEs with energies $\leq$ 30 eV contribute about 90% to the total electron yield. The SEs are emitted with a large angular spread. Accelerating them to the energy of 3 - 4 keV the dispersion is only partly reduced, therefore after the deflection to 180°, by means of a magnetic field, not all the SEs will reach the detector surface, and those which will reach it, will have certain dispersion in energy and position. In the crossed electric and magnetic fields the electrons move along isochronous trajectories and the position of incidence on the foil is reflected one to one onto the MCP. Any residual angular dispersion in the plane of the bend can be reduced by the use of a collimator, located at the 90° bend position of the SEs trajectories (ZE1). Such a quarter-turn collimator can improve the time and position resolution of the device, but may cause certain decrease of the detection efficiency, especially in the case of low ionizing ions.

The detection efficiency of a MCP depends on the energy of SEs. This dependence was studied by several authors (e.g. BO1, WE1). The efficiency reaches a plateau for electron impact energies above 350 eV. In the case of a 2π secondary electron trajectory from the foil to the MCP surface in crossed electric and magnetic fields (Fig.1), the SEs would have energies close to zero and the detection efficiency would be extremely low. A very often used solution is the displacement of the MCP relative to the foil as it is shown in Fig.7. The displacement by 2 - 3 mm, according to the design of the apparatus, will allow the SEs to have impact energies above 350 eV. The displacement will cause only a small fluctuation of the SEs transit time.

As target foils mostly thin carbon foils ($\geq 20\mu g/cm^2$) are used. For higher strength the carbon foil can be evaporated on a thin Formvar or cellulose nitrate foil. The number of SEs emitted when an ion traverses a foil is proportional to the specific energy loss of the ion in the given media. With increasing atomic number Z the efficiency of the detecting system approaches unity but with increasing energy the efficiency will drop. An extrapolation in ref. (GA1) gives for ^{12}C beam at 45 MeV/u on a carbon foil an efficiency of $< 40\%$.

3. Electron Detecting System

Channel electron multiplier plate: The mostly used microchannel plate electron multipliers have channel diameters of 10 - 25 μm. The insensitive part of the MCP front face is amounting about 50% or even more for some types of MCPs. This has two consequences. First, about half of the SEs do not penetrate into the MCP channels and do not create electron avalanches. Second, ternary electrons are emitted from the insensitive part of the MCP. The ternary electrons, after a small loop will hit the channel plate again and thus they produce a second signal, delayed a few nanoseconds. This is the case in detectors, working with accelerating grids, where the SEs after acceleration move only in a magnetic field. This problem can be solved by placing a suppression grid in front of the channel plate (GRID 2 in Fig.2) (ZE1). The grid has a positive potential with respect to the MCP surface, therefore the ternary electrons are accelerated away from the MCP.

The electron detection system consists of two MCPs. The system of two MCPs assembled in a Chevron configuration exhibits a high gain because of the multiplicity of channels excited in MCP2 by a single channel in MCP1 (Fig. 4). The separation of the two MCPs can be chosen from about 0.1 mm to more than 3 mm. At a very small distance the position resolution will be improved, but the gain of the second MCP will be smaller.

If an accelerating potential is applied between MCP1 and MCP2, the angular spread of electrons from MCP1 will be reduced and fewer channels in MCP2 are excited. At 100 V accelerating potential the number of channels in MCP2 excited by one channel in MCP1 is reduced by about a factor of 3 (WI1). Higher acceleration potential has almost no effect on the final gain. For high current gain no potential should be applied. On the other side an accelerating voltage between the Chevron MCPs improves the rise time of the output pulses.

Dead time. After a channel "fires", the charge in the channel walls must be replenished. The channel recovery time is about 10 - 20 ms. The channels operate more or less independently, therefore the effective dead time of an MCP is of the order of $10^{-7} - 10^{-8}$s if the incident flux is uniformly distributed over the active area and no single channel is excited more frequently than once every 10 ms. With uniformly distributed incident particles at random count rates up to 2×10^6 s^{-1} no serious efficiency degradation was observed (WI1).

Signal: The signal rise time is typically 400 - 600 ps, but probably less than 100 ps would be achieved. The amplitude varies typically between 0.2 and 1.0 V, depending on the applied voltage and the number of emitted SEs. The collecting voltage between the anode and bottom MCP surface is not critical, a setting above 50 V is sufficient as it was observed by E.Weissenberger et al. (WE1).

Timing signal and time resolution: The timing signal can be taken either from the anode or from the last channel plate electrode, if the anode is needed for position determination. In the last case a pulse of somewhat reduced quality is derived. Excellent time resolution, 70-100 ps in the case of a small foil and MCP size (few cm^2) were achieved (KR1). The transit time of SEs between the target foil and MCP should be minimized in order to reduce transit time uncertainties. For this the foil to MCP distance should be minimized and the magnitude of both fields should be as high as possible.

The time dispersion in the SEs flight times has several sources. The basic source is the velocity spread of the SEs as they are knocked out of the foil. The initial velocity v_0 of the SEs is about $\approx 10^8$ cm/s and according to Bowmann et al (BO1) the value of the time spread Δt will depend on the applied electric field E

$$\Delta t = \frac{m v_0}{e} E^{-1} \tag{9}$$

At the used values of E of about 1 to 2 kV/cm the time fluctuation will be of the order of a few tens of ps.

In the case of large size detectors variations in signal transport time across the anode plate can contribute significantly to the time spread. To correct for it, an anode with a specially shaped front surface can be used, to exploit the different time-of-flights of electrons from the last channel plate to the anode surface (Fig.5). This compensates different transport times of the pulse through the anode. The back side of the anode can be formed as a 50 Ω cone, to eliminate reflections caused by the impedance jump between the flat anode and 50 Ω output coaxial cable. The kinematic equations used to calculate the shape of the anode surface, are given in details in ref. (KR1). The difference Δd in the anode front shape can be calculated using a simple equation

$$\Delta d = 10^{-3} r \sqrt{V} \tag{10}$$

where r is the radius of the anode (center to edge distance in the case of rectangular anodes), given in millimeters and V is the voltage, applied between the anode and last MCP surface, given in Volts. For the MCP detector, described in ref. (KR1) such an anode should correct for up to 70 ps of time resolution.

4. Position measurement

Charge division principle. For the x- and y-position measurement the charge division principle can be used which is well known from position sensitive surface barrier detectors. For this purpose the anode of the channel plates is subdivided into parallel strips, for example 1 mm wide, which are connected together by a delay line. Position resolution of 1.3 mm was achieved by F.Busch et al. (BU1) using 2 mm wide anode strips and 15 x 50 mm^2 overall sensitive area.

R.E.Renford et al. (RE1) used for position determination an anode, made from a thin carbon resistor layer. The position resolution of the MCP - anode system, measured without magnetic deflection, by direct irradiation with alpha particles, was 0.35 - 0.4 mm. The position resolution with magnetic deflection of the SEs was 0.5 mm for alpha particles and 0.4 mm for heavier ions. A similar system used by H.Ikezoe et al. (IK1) provided position resolution of 0.3 mm.

X and Y anode wire grids and strips. H.Keller et al. (KE1) developed a position readout anode using also the charge division principle. The anode is divided into parallel strips which are connected by a delay line. One strip has a width of 1.5 mm and consists of 5 wires. The width of one strip is chosen according to the calculated diameter B of electron space charge, reaching the anode wire grid

$$B = (\sqrt{1 + 0.067U} - 1)60d/U, \tag{11}$$

where U is the MCP2-anode voltage in Volts and d is the MCP2-anode distance in mm. The capacity coupling between the MCPs, and especially between the last

MCP and anode, can strongly deform the output signal and significantly decrease the time resolution. To prevent that, high frequency grounding of each MCP was made with four 5 pF capacitors, circularly surrounding the MCPs. The time delay is directly related to the position of the incoming particle. The two-dimensional position information is obtained from two crossed grids and a reflector plate behind. The obtained resolution is 0.25 mm and can be improved.

The average amplitude of the anode signal may achieve $\approx$ 1 Volt and a rise time $<$ 1 ns. This should by enough to use, instead of wires, crossed x-, and y-strips isolated each to other with a thin layer of dielectric material. For 1 mm wide strips, using 2 μm thin dielectric layer (dielectric constant $\epsilon_r \approx 3$) between the x- and y-strips the capacity of one xy area (1 mm^2) is C $\approx$ 13 pF and for 0.5 mm wide strips C $\approx$ 3 pF. Even the last value is large enough to obtain a satisfactory output signal from both, x- and y-strips.

Desired electric and magnetic field homogeneity: From the expressions given above we can determine, that for example at a lateral displacement of y = 8 cm for the position sensitivity of $\pm$ 1 mm the inhomogeneity of the electric field should be $\leq$ 1.3% and that of the magnetic field $\leq$ 0.7%. For position sensitivity of $\pm$ 0.5 mm the same quantities should be $\leq$ 0.6% and $\leq$ 0.3%, respectively. The required homogeneity of the electric field can be easily obtained. Using field correction equipotential rings or frames the field distortion can be acceptable also at the edges of the effective detector volume.

To construct a magnet with a desired field homogeneity is also possible. The final effect of inhomogeneities may remain in limits also in the case, when local field inhomogeneities exceed the desired limit. J.D.Bowman (BO1) used a permanent magnet assembled from 140 small permanent magnets and the resulting magnetic field is homogeneous to better than 0.5% in the whole volume of the transport system. Using permanent magnets and Rose shims, magnetic field homogeneity of $\pm$0.1% is reported (KR1). The use of electric magnets rather than permanent magnets has the advantage of flexibility, allowing a change of the acceleration voltage whenever desired.

5. Detection efficiency

The detection efficiency ϵ_d depends on the effective charge and energy of the ions, penetrating the foil. For low energetic alpha particles (E = 1 MeV/u) $\epsilon_d \approx 75\%$; for low energetic heavy ions $\epsilon_d \approx 100\%$. To achieve high detection efficiency for high energetic light ions, the detector foils have to be covered with a thin layer of material, which has a high coefficient of secondary electron emission. If the emitted SEs are accelerated by a grid, 1 - 3 mm away from the target foil, this causes a reduced transmission (e.g. 95% (RE1)) of the detected ions and also the ion beam may have an increased low energy tail.

6. Background

The background or noise of a MCP itself is relatively low. It depends on the ^{40}K concentration in the glass and on the intensity of laboratory gamma rays. The total pulse rate of a MCP unit due to cosmic rays, ambient laboratory radioactivity and internal effects, is on the order of 0.2 counts/cm^{-2}s^{-1} (PA1). The main source of background signals are thermal electrons, emitted from the target foil and also those thermal electrons, emitted from other surfaces, which can be accelerated to the MCP surface. The transition of ions through a foil causes together with the emission of SEs also emission of X-rays. The sensitivity of MCP to X-rays is low, the X-ray detection efficiency does not exceed a few percents. If the design of the detector allows the X-rays to reach the MCP surface, they will cause additional background pulses.

7. Advantages and disadvantages of foil - MCP detectors

As advantages we can consider:
1. High count rate, the estimated maximum is about of $10^5 - 10^7$ s^{-1};
2. The possibility to use for fast timing, for small size timing units about 100 - 300 ps time resolution is achievable;
3. Fast high amplitude output signal, the signal rise time is about 400 - 500 ps or even less;
4. Very small amount of material in the beam, only 20 μg/cm^2 in the case of self-supporting carbon foils;
5. In the case of position sensitivity there is a possibility to detect many ions simultaneously;
6. Good spatial and double track resolution (0.2 - 0.3 mm).
The disadvantages:
1. Low detection efficiency for high energy light ions;
2. Large dynamic range of the output signals, resulting in amplitude-to time walk of the CFD in the case of ions with very different SE yield;

8. The possibility to use foil-MCP detectors for high energy ions

The development of heavy ion accelerators and ECR ion sources made it possible to realize many new physical experiments with intermediate and high energetic ions. Some of these experiments require very precise determination of momentum distribution, in spite of the energy region 0.1 - 1.0 GeV/u or even more. To determine the trajectories of high energetic ions, arrays of xy-coordinate detectors are used. There are several types of detectors, which are able to give position information: multiwire proportional counters, time projection proportional chambers, parallel plate avalanche counters, scintillation detectors, silicon detectors and foil-MCP detectors. In the case of multiwire proportional counters the presence of many layers of wires in the ions trajectories become critical for some experiments. To decrease the mo-

mentum spread and scattering effects, caused by wires, thin wireless, homogeneous coordinate detectors should be used. Such types of detectors are in the process of development on the basis of GaAs, but their thickness determinate their use mainly in the energy region above 1 GeV/u. One of the possibilities is to use foil-MCP position sensitive detectors. The properties of these detectors, described above, fulfil all the desired parameters, except the detection efficiency for weakly ionizing high energy light ions. For light ions with energies above a few tens of MeV/u the number of emitted SEs will decrease below the value, needed for 100% detection efficiency.

Transitory secondary electron emission (TSEE). According to the known experimental data a MCP detector will have a detection efficiency close to 100 % when the number of SEs, emitted from the target foil, will be at least 10 to 15. SEs are emerging from a mean depth of about $0.01\mu m$, therefore the effective carbon foil thickness is only a few $\mu g/cm^2$ (GA1, SA1). This means that in the case of unsufficient number of emitted SEs the larger thickness of the foil does not help. In the case of particles, creating in the foil less SEs than the critical value, an internal multiplication process can be applied. Such a multiplication process is going on in the case of TSEE. The investigation of TSEE was started in the sixties, using target foils coated with porous alkali halides (GO1, GO2, LO1, LO2, ST2). A new progress in TSEE was reported in the eighties by C. Chianelli et al. (CH1) and R.L. Kavalov (KA1). The primary layer of the TSEE detector must produce at least one SE for each penetrating particle. The second porous dielectric layer multiply the SEs. Multiplication effect can be created in such porous alkali halies as KCl, CsI or MgO, having a density of some few percents of the bulk density. The mechanism of TSEE from a low density dielectric layer is similar as in channel electron multipliers or MCP. The coefficient of secondary electron emission (SEE) is more than 100 times higher than for normal density substances. SEs, emitted from a low density layer are multiplied in the pores of the dielectric by an applied high intensity electric field (Fig. 6).

There are only a few experimental works on TSEE. To increase the secondary electron yield, H.L. Seifert et al. [SE1] have evaporated a thin layer of CsI onto the basic target foil. For alpha particles 25 $\mu g/cm^2$ CsI coating improved the detection efficiency from $\approx$ 75 to 98 % and reduced the dynamic range of the anode signal by a factor of $\approx$ 10. According to the authors at least four times more SEs are produced from CsI coated foils as compared to those without CsI.

Using KCl or MgO low density foils R.L.Kavalov et al. (KA1) reported 100% detection efficiency for 5.48 MeV alpha particles and about 60% detection efficiency for 1 - 2 MeV electrons. The MgO layer, 100 $\mu g/cm^2$, with relative density $\rho/\rho_0 \approx 0.6\%$ ($\rho_0 = 3.65$ g/cm^3) was deposited onto a Nickel fine mesh (88%). The multiplication of SEs in the porous dielectric is caused by a strong electric field, $E \geq 10^4$ V/cm, created between the basic electrode and a grid, spaced at 0.5 mm distance from the layer surface. Increasing the field strength from 10^4 V/cm to 1.5×10^4 V/cm, the number of SEs from α particles increased from 70 to 120. This is more than 10

times higher than from carbon foils. The disadvantage of this method is the presence of the supporting grid and the accelerating grid, decreasing the transmission. The system can be improved supporting the dielectric layer by a thin conducting foil.

By C. Chianelli et al. (CH1) for TSEE investigation CsI has been chosen because of high secondary emission and low hygroscopic properties. As the primary layer 45 $\mu g/cm^2$ self-supporting alumina (Al_2O_3) foil was used on which 1300 $\mu g/cm^2$ (120 μm) porous CsI layer was evaporated having a relative density of 2.5 % of the bulk density. This layer had a structure of 10 to 50 nm CsI whiskers. By 5.48 MeV α-particles about 100 SEs were emitted from the CsI layer. For low ionizing electrons of energies $\geq$ 1 MeV the average number of emitted SEs is $\overline{n} = 4$. Constant SEE yield was obtained at the electric field strength above 14 kV/cm. The SEE yield is time dependent. Immediately after applying the high voltage, the yield is very high, but exponentially decreasing, reaching a constant value after 2 - 3 hours. To keep the yield at a very high value, attempts were made to apply a periodic electric field, synchronized with the time structure of the accelerated ion beam.

An additional amplification factor of 6 or 7 was obtained when the accelerated secondary electrons, emerging from the porous CsI layer hit the back surface of another detector. This detector was made of a self-supporting 45 $\mu m/cm^2$ (100 nm) alumina (Al_2O_3) foil, aluminium layer (30 nm) and a bulk CsI layer of 60 nm, acting as a secondary emitter. Because of the high electric field intensity, applied on the porous CsI layer, the vacuum have to be lower than 10^{-5} Pa

To determine the energy range of high energy ions, where foil-MCP detectors would work with detection efficiency close to 100%, the SEE yield should be known as a function of Z and energy of the ions. There are almost no experimental data on SEE yields and energy distribution from foils in the intermediate and high energy range. But from the data, given by H.-G. Clerc et al (CL1) it is evident, that the measured SEE yield is in good agreement with the differential energy loss in carbon foils for the investigated ^{4}He, ^{16}O, ^{32}S and ^{127}I ions.

9. Large area TOF detectors for low energy evaporation residues.

Nuclear reactions near the Coulomb barrier create evaporation residues (ERs) - ions with kinetic energies as low as 0.05 - 0.2 MeV/u. In advanced experimental set-ups the ERs, after passing through a kinematic separator, are detected with an array of strips of position sensitive Si-detectors. To distinguish between signals, created by ERs and target- and projectile-like ions, a time-of flight detector system is used in front of the Si-detector array. The TOF detectors determine the velocity distribution of the ions, and together with the corresponding energy signal from the Si-detector a two-dimensional energy - velocity spectrum can be created, where as a rule, the mentioned three groups of ions are separated each of other. With respect to the low energy of the ERs, the TOF detectors must have as little material in the trajectory of the ions as possible, to minimize multiple scattering, energy straggling and energy

loss of particles. For very low energy evaporation residues, created in asymmetric reactions, the energy loss would be critical. Thus the use of silicon detectors, or other type of detectors with an overall thickness above 200 -300 $\mu g/cm^2$ as TOF detectors is not possible. Different types of foil-microchannel plate TOF detectors are used in the case of low energy ions, because in this type of detectors the ions have to penetrate only 10 to 30 $\mu g/cm^2$ thick foils.

9.1. TOF detectors for the velocity separator SHIP

For the purposes described above a large size TOF START-STOP detector unit was developed for the use at the velocity separator of recoiled evaporation residues SHIP (MU1), operating on the beam from the UNILAC linear accelerator of GSI Darmstadt. The position sensitive Si-strip detector array as the analyzing detector of SHIP has an effective size of (80×35) mm^2. The beam profile of the evaporation residues behind the SHIP requires to use a TOF detector system, having a very large effective area. For the START detector we used a carbon foil of (94×77) mm^2 effective area and for the STOP detector 94×55 mm, respectively. The foils have thicknesses of 20 to 30 $\mu g/cm^2$. The available large size MCPs have effective areas of (94×77) mm^2 (Hamamatsu, Japan), (93×75) mm^2 (Galileo, USA) and (80×64) mm^2 (Russia). The TOF detectors can work with all the above mentioned types of MCPs. The effectively used areas are (85×70) mm^2 for the Galileo and Hamamatsu MCPs and (80×64) mm^2 for the Russian MCPs, respectively.

The channel-plates were used in a standard Chevron arrangement (Fig.7) The distance between MCP1 and MCP2 is 2 mm and the anode is mounted 3 mm behind MCP2. Because of the large size, anodes with shaped front surfaces were applied. According to eq.(2), the shaped anodes should correct for up to 100 ps of electron transport time. The housing of the channel-plate units were made from stesalit, a good insulator and high vacuum (10^{-5} Pa) material. The size of the frames was minimized to avoid any significant field distortion. For fine setting the voltage on the MCPs, basic and accelerating electrodes, independent stabilized high voltage power supplies were used. The large rectangular opening in the acceleration plate, (94×77 mm^2), should cause serious field distortion, therefore it is covered with an additional thin carbon foil. To eliminate field distortion at the edges of the plates, field correction frames were used, which were held at the chosen equipotential levels by a voltage divider chain of resistors. The schematic view of the whole TOF device is shown in Fig.8.

The emitted SEs are accelerated in a homogeneous electrostatic field, created between the two parallel plates, distant 38 mm, and bend to 180° in a homogeneous magnetic field to the surface of MCP1. The magnetic field is created by an electromagnet. Because of the slightly inefficient cooling of the magnet coils, only by radiation in the vacuum, the magnets are cooled. The SEs lateral displacement is 86 mm for the START detector and 79 mm for the STOP detector. The calculated amplitude of the cycloidal trajectories is 27 mm for the START detector and 25 mm

for the STOP detector. To let the SEs hit the surface of MCP1 with an energy of $\geq$ 350 eV, the surface of MCP1 is shifted 3 mm into the electric field and the voltage of MCP1 is adjusted to the given equipotential level. Both, START and STOP detectors, are mounted on a movable support, which gives the possibility to change the TOF basis from 13 cm to 38 cm (42 cm) externally, by a vacuum feedthrough, and to get the whole TOF unit, mounted on one rectangular metal plate, into the vacuum box.

The electronic setup for the time measurement is shown in Fig.9. All the used electronic units are CAMAC/NIM modules and are commercially available. Registered are all the three combinations of Si-detector energy signals (Si) versus time-of-flight signals: Si - START foil (TE - TF1), Si - STOP foil (TE - TF2) and Si - (foil1 - foil2) (TE - T(F1-F2)). From the START and STOP detectors TOF bit signals are given to the Camac read out system.

The counting efficiency of the whole TOF detector system is $\geq$ 99% (preliminary data). Due to the large size of the C-foils, especially in the START detector, no ERs are absorbed on their way from the SHIP output magnet to the active part of the Si-strip detector array.

For heavy evaporation residues from fusion reactions, having masses $\geq$ 200 amu and energies from about 5 MeV to 70 MeV, the typical times of flights (at 50 cm TOF basis) are about 70 to 250 ns and will differ by about 0.2 to 1 ns for ERs different by one mass unit. With foil-MCP detectors having the size $\geq$ 50 cm^2 it is probably not possible to achieve time resolution $\leq$ 200 ps (see Tab.3). At a preliminary measurement $\leq$ 750 ps time resolution was achieved for the whole TOF system of SHIP with ^{241}Am alpha particles and about 700 ps with 12 MeV ERs. According to our estimation the time resolution of the SHIP TOF system can achieve at optimum working parameters and after some improvements about 300 - 400 ps. It would allow to determine the masses of most of the investigated ERs. But no effort was made to improve the time resolution of the TOF system, because the limitation of the mass determination is caused by the energy determination with the silicon detector. The pulse height defect in the silicon detector in the case of heavy ERs achieves many percents and corresponds to many mass units. The role of the TOF detectors is to distinguish the ERs, created in complete fusion reactions, from target like transfer reaction products and scattered projectile-like ions, which are the most significant background components in the spectra of ERs. For this purpose 1 ns time resolution of the TOF system is acceptable. The most important role of the TOF systems at heavy element fusion experiments is to help to distinguish between signals from the alpha-decay chains of ERs, implanted into the Si-end detector array, and signals created by particles, impinging on the Si-detector. For this purpose the TOF detector signals and the signals from the Si end detector array are in anticoincidence condition. An example of a two-dimensional TOF spectrum is given in Fig.10., where the scatter plot of the time-of-flight of ions between the START and STOP foils is plotted versus the ions energy, measured in the reaction of ^{58}Fe + ^{208}Pb at SHIP.

The complete fusion 1n-channel of this reaction, leading to the isotope of $^{265}108$, is only a few tens of picobarns, therefore the role of the TOF detectors as an anticoincidence unit is substantial.

9.2. TOF detectors for the electrostatic separator VASSILISSA

A large area TOF detector system was developed for heavy element fusion experiments also at the electrostatic separator VASSILISSA (YE1) at Flerov Laboratory of Nuclear Reactions, JINR Dubna. The detecting system of the separator consists of two timing detectors and an array of position sensitive silicon strip detectors. The chosen timing detector system is based on the type, shown in Fig.2, but some special features were developed which enable to improve the performance of such a system.

The trajectories of SEs in such a quarter-turn timing detector are not isochronous as it is shown in Fig.2. Consequently the transition time of a SE depends on the position, where it was created by an ion, passing through the target foil. The influence of nonisochronous trajectories on the time resolution is eliminated, when identical START and STOP timing detectors are used, as it is shown in Fig.11. In the area near the focal plane of the separator, where the TOF detectors are installed, the beam of reaction products is nearly parallel and fulfil the condition for isochronous trajectories in both detectors. (for instance flight paths E1-E2, and E1'-E2' in Fig.11.). Due to the focusing action of the 90° deflection system, the resulting image will be reduced in size and MCPs with smaller dimensions can be used.

As the emitter of SEs a mylar foil of about 20- 30 $\mu g/cm^2$ thickness has been used, covered by vacuum evaporated gold layer of 10 -20 $\mu g/cm^2$ thickness. The effective diameter of the foil is 82 mm ($\approx$ 50 cm^2 effective area). To use the possibility to collect the emitted SEs from both sides of the foil two accelerating grids can be used at each foil (START and STOP) as it is shown in Fig.12.

The deflecting electro-magnets have a size of $90 \times 180 \times 20$ mm, the created magnetic field has a calculated uniformity of 0.1%. A simplified view of the timing detector is given in Fig.13. For the simplicity the coil, winded on the external C-shaped part of the magnet, is not shown.
The grounded acceleration grids are 5 mm apart from the foil. The transparency of each grid is 97.5%, yielding a total transparency for the whole START-STOP system of about 90%.

Zero potential shielding grids were installed also in front of the MCP units to suppress the defocusing influence of the MCP electric field on the SE trajectory. As the output electrode a cone-shaped 50 Ω impedance anode was used to match the impedance of the output cable.

Using ^{226}Ra alpha particles as projectiles and detecting SEs only from one side of

the foils, 440 ± 40 ps time resolution was achieved at 80% counting efficiency. If SEs were detected from both sides of the foils, the time resolution was 600 ± 40 ps at a counting efficiency of about 90%. With 10 MeV evaporation residues as projectiles, 500 ± 40 ps time resolution was achieved at 99.99 % counting efficiency when SEs were detected only from one side of the foils. The detection of SEs from both sides of the foils leads to ≥ 99.99 % detection efficiency. The time resolution in this case was not determined. The data on counting efficiencies given above do not include the losses, caused by the accelerating grids.

As it was mentioned, one of the most important applications of a TOF system is to use it in anticoincidence condition between pulses from TOF detectors and from the Si-detector. The probability p_{ac} to get an anticoincidence signal from the whole TOF system of four detectors is given as follows:

$$p_{AC} = 1 - (1 - p_S)^4, \tag{12}$$

where p_S is the probability to register the ion by any single MCP detector. In the case of heavy ion registration the value of p_S is close to 1, therefore the efficiency of the anticoincidence condition (12) is very high. In fact, for an effective application of the anticoincidence condition it is not necessary to register an ion with all MCP detectors.

More details about the TOF detector system at the electrostatic separator VASSILISSA are given in (AN1).

10. Conclusion

Long term operation of both TOF detector systems, at SHIP and VASSILISSA separators have proved, that foil-MCP type timing detectors can manage ion beams with spot sizes ≥ 50 cm^2. The achieved time resolutions enable to distinguish ERs from target-like and scattered nuclei in a wide range of projectile - target combinations. The registration efficiency of the VASSILISSA TOF system, collecting SEs from both sides of the target foils, is ≥ 99.99%, but the transparency of the system is only 90%. The registration efficiency of the SHIP TOF system, collecting SEs only from one side of the target foils, is ≥ 99% at ≈ 100% transparency.

The transparency of the VASSILISSA TOF system can achieve ≈ 100% using accelerating field plates and foils, like at SHIP, instead of grids, accelerating the emitted SEs. This solution has a limitation. At very low ER energies, of the order of a few MeV, the additional foils, covering the holes in the accelerating electrodes, can cause serious absorption of the ERs.

The registration efficiency of the SHIP TOF system can reach ≥ 99.99% collecting the SEs from both sides of the target foils. Because of the space limitation in the vacuum chamber, in this case quarter-turn SE trajectories from the target foil to

MCP should be used.

References

(AN1) A.N.Andreyev et al., NIM (to be published).
(BO1) J.D.Bowman and R.H.Heffner, NIM 148 (1978) 503.
(BU1) F.Busch et al., NIM 171 (1980) 71.
(CH1) C. Chianelli et al., NIM A 273 (1988) 245.
(CL1) H.G. Clerc et al., NIM 113 (1973) 325.
(DE1) G. D'erasmo et al., NIM A 234 (1985) 91.
(DE2) C.C.Dedman et al., NIM B 24/25 (1987) 366.
(FR1) H.J. Frischkorn et al., NIM 214 (1983) 123.
(GA1) A. Galindo-Uribarri et al., NIM A 301 (1991) 457.
(GO1) G.W. Goetze, in Advances in electronics and electron physics, Ac.Press, N.Y., 1962, Vol.16, p.145.
(GO2) G.W. Goetze, A.M. Boerio and M. Green, J.Appl.Phys. 35 (1964)482.
(HE1) R.D. Heil et al., NIM A 239 (1985) 545.
(HE2) F.P. Heßberger et al., GSI Scientific Report 1982, p.223.
(IK1) H. Ikezoe et al., NIM 196 (1982) 215.
(KA1) R.L. Kavalov et al., NIM A 237 (1985) 543.
(KE1) H.Keller et al., NIM A 258 (1987) 221.
(KR1) R.H. Kraus et al., NIM A 264 (1988) 327.
(LO1) M.P. Lorikian et al., NIM 122 (1974) 377.
(LO2) M.P.Lorykian and N.N. Trofimchuk, NIM 149 (1977) 505.
(MU1) G.Münzenberg et al., NIM 161 (1979) 65.
(PA1) W. Parkes et al., NIM 121 (1974) 151.
(PE1) J.P. Pearson et al., NIM A 325 (1993) 578.
(PF2) K.E. Pferdekämper and H.-G. Clerc, Z.Phys A 275 (1975) 223.
(PF3) K.E. Pferdekämper and H.-G. Clerc, Z.Phys A 280 (1977) 155.
(RE1) R.E.Renford, H.Noll and K.Sapotta, NIM 185 (1981) 157.
(SE1) H.L. Seifert et al., NIM A 292 (1990) 533.
(SE2) H. Seiler, Z.Angew.Phys. 22 (1976) 249.
(ST1) E.J. Sternglass , Phys.Rev. 108 (1957) 1.
(WE1) E. Weissenberger et al., NIM 163 (1979) 359.
(WI1) J.L. Wiza, NIM 162 (1979) 587.
(YE1) A.V.Yeremin et al., NIM A 350 (1994) 608.
(YO1) Keiko Yuasa-Nakagawa et al., NIM (1991) 538.
(ZE1) A.M. Zebelman et al., NIM 141 (1977) 439.

Table 1. Number of emitted SEs in the forward and backward hemispheres from 10 $\mu g/cm^2$ carbon foil by alpha particles and light fission fragments from ^{252}Cf source (data from PF3)).

Projectile	Alpha particles 0.48 MeV/u	Alpha particles 1.5 MeV/u	Light fission fragments 0.93 MeV/u
2π forward			
SEs < 230 eV	5.7 (89%)	2.4 (86%)	139 (58%)
SEs > 230 eV	0.7 (11%)	0.4 (14%)	99 (42%)
2π backward			
SEs < 230 eV	3.0 (98%)	1.9 (96%)	75 (87%)
SEs > 230 eV	0.09 (2%)	0.07 (4%)	11 (13%)
Mean energy of SEs, eV	60	100	290

Table 2. The total number of emitted SEs in both, forward and backward directions, from a carbon foil for different ions.

Projectile	Energy (MeV/u)	Average num. of SEs (4π)	Ref.
^4He	0.48	9.5	PF3
	0.78	8.1	CL1
	1.50	4.8	PF1
	1.52	5.5	CL1
	2.2	3.9	
^{16}O	0.11 - 1.84	$\approx$ 50	CL1
^{32}S	0.23 - 1.35	$\approx$ 95	CL1
^{127}I	0.08	83	CL1
	0.16	124	
	0.27	163	
Light fission fragments from ^{252}Cf	0.93	324	PF3
Z_{ev} = 43	$\approx$ 0.75	192	CL1
Heavy fission fragments from ^{252}Cf			CL1
Z_{ev} = 55	$\approx$ 0.35	170	

Table 3. Comparison of some parameters of foil - MCP detectors.

Detector type, size cm^2	Incident ions MeV/u	Time resol. ps	Position resol. mm	Detection efficiency %	Max. count rate s^{-1}	Ref.
1.3	6.5 ^{16}O	90				ZE1
	2.2 α	150		57 (65)		
2.7	1.35 α	68		83		KR1
10		109		75		
8	1.4 α	200	0.6			RE1
	4.8 ^{40}Ar	175	0.4			
	5.4 ^{208}Pb		0.4			
CF,small	1.37 α	230		75	$\approx 10^6$	BO1
small		500	0.25			KE1
3.4	1.37 α	120	0.3			IK1
small	^{252}Cf ff	115		99.9		WE1
EM	1.37 α	240		65		HE1
$\approx$10	^{252}Cf ff			90		
EM	1.37 α	150		72		DE1
small	1-18 MeV light ions			60-100		
					10^5	PA1
		200				SE1
EM	2 α	150	1.3			BU1
7.5	1.4 Pb	to 200		$\approx$100		
TSEE	1.12-1.87 α	250		100		KA1
small	1-2 MeV electrons			60		
TSEE	540 MeV protons	450		$\geq$ 95		CH1
EM	1.2 α, 0.4 ^{197}Au	$\approx$550		$\approx$ 100		HE2
18	4.8 ^{58}Ni	250				
	1.4 ^{208}Pb, ^{142}Nd	$\approx$190				
CF	4.8 MeV α	600		90$\times$0.9		AN1
50	10 MeV ERs	500		99.99$\times$0.9		
CF	4.5 MeV α	$\leq$750[a]		77		This
55	12 MeV ERs	$\leq$700[a]		$\geq$ 99		work

CF - crossed electrostatic and magnetic fields
EM - electrostatic mirror
TSEE - transitory secondary electron emission
a - preliminary data

Captions to figures

Fig.1. The schematic view of the foil-MCP detector, operating in crossed electric and magnetic fields. E - electric field B - magnetic field, e^- - secondary electron trajectory.

Fig.2. The schematic view of the quarter-turn foil-MCP detector operating in a homogeneous magnetic field, with accelerating wire GRID1 and suppression GRID2.

Fig.3. The schematic view of the foil-MCP detector, operating on the principle of an electrostatic mirror with 90° bending. G1 - accelerating grid, G2 and G3 - electrostatic mirror grids, e^- secondary electron trajectory.

Fig.4. Chevron type MCP detector system consisting of two MCPs.

Fig.5. Shaped anode surface to eliminate different transport times of signals through the anode to the output cable.

Fig.6. Transitory secondary electron emission from a low density dielectric foil. CF - primary carbon foil, AH - very low density alkali halide layer (CsI), G - accelerating grid.

Fig.7. The arrangement of a foil-MCP detector units at SHIP. FCF - field correction frames.

Fig.8. Schematic view of the large area TOF detector system for the SHIP kinematic separator. FCF - field correction frames.

Fig.9. Block-scheme of the electronic setup for the time measurement by the SHIP time-of-flight detector system. FTA - fast timing amplifier, CFD - constant fraction discriminator, DL - delay line, TAC - time-amplitude-convertor, ADC - amplitude-digital-convertor.

Fig.10. Two-dimensional Time-of-Flight - Energy scatter plot, measured in the reaction of ^{58}Fe + ^{208}Pb at the kinematic separator SHIP.

Fig.11. Quarter-turn TOF detectors with accelerating grids, detecting SEs from both sides of the foils. Trajectories E1 - E2 and E1'- E2' are identical.

Fig.12. The schematic view of one TOF detector unit, used at the electrostatic separator VASSILISSA.

Fig.13. A simplified view of the timing detector. For simplicity the coil, winded on the C-shaped part of the magnet, is not shown.

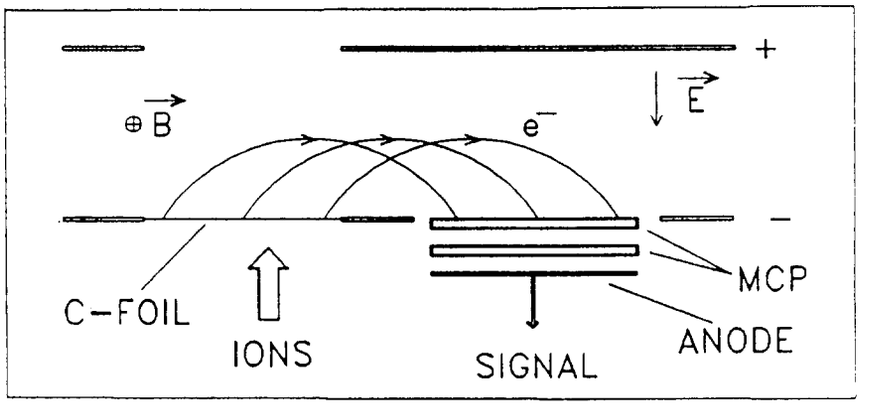

Fig1. The schematic view of the foil-MCP detector, operating in crossed electric and magnetic fields. E - electric field, B - magnetic field, e¨ secondary electron trajectory.

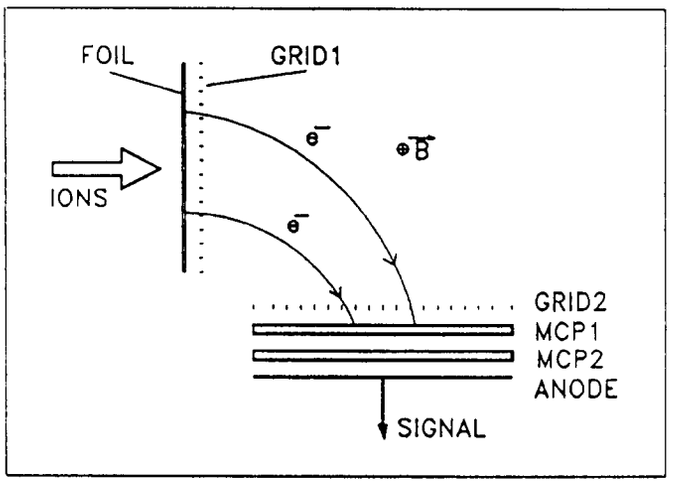

Fig.2. The schematic view of the quarter-turn foil-MCP detector, operating in a homogeneous magnetic field, with accelerating wire GRID1 and suppresion GRID2.

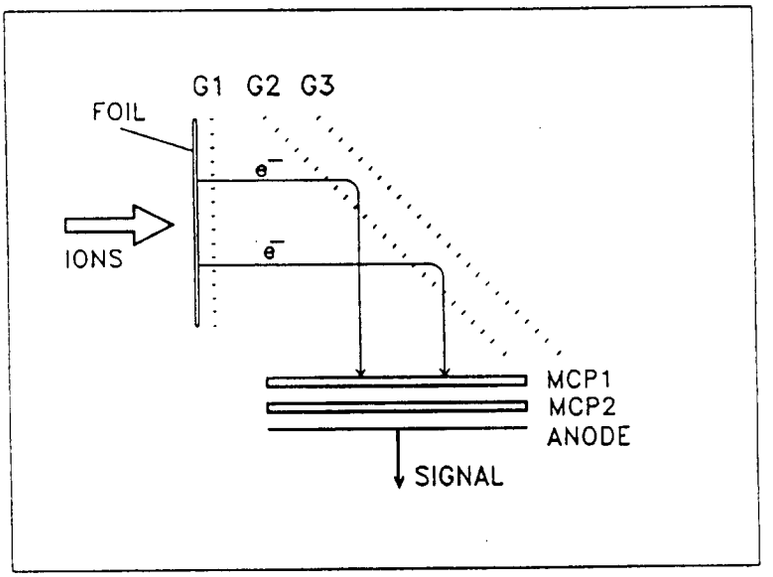

Fig.3. The schematic wiew of the foil-MCP detector, operating on the principle of an electric mirror with 90^0 bending. G1 - accelerating grid, G2 and G3 - electrostatic mirror grids, e¨ secondary electron trajectory.

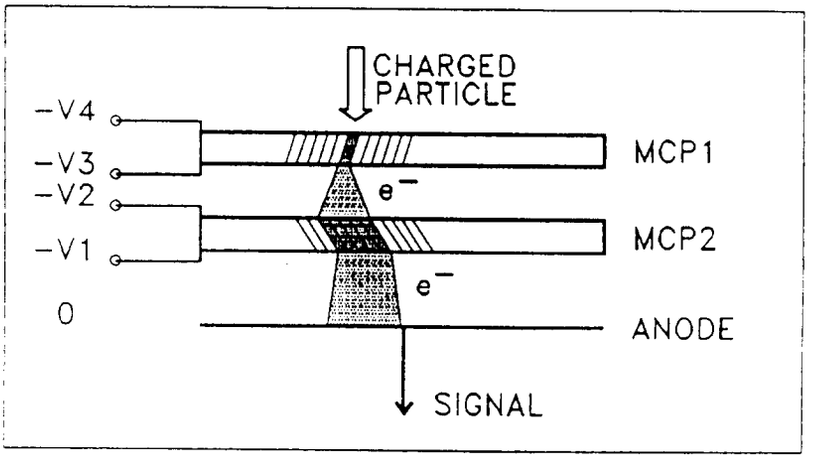

Fig.4. Chevron type MCP detector system consisting of two MCPs.

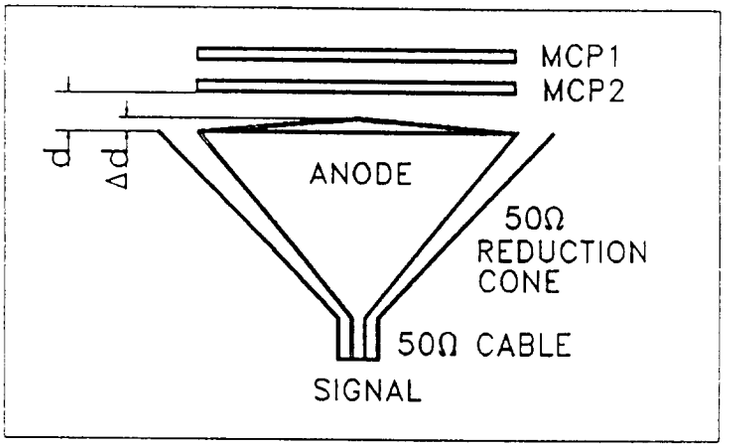

Fig.5. Shaped anode surface to eliminate different transport times of signals through the anode output cable.

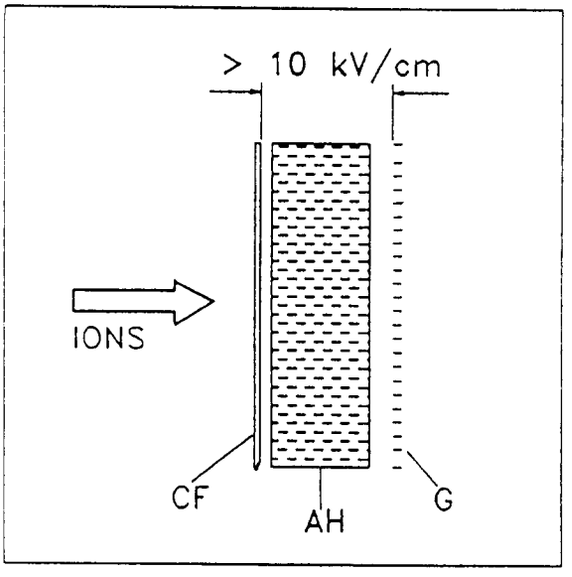

Fig.6. Transitory secondary electron emission from a low density dielectric foil. CF - primary carbon foil, AH - very low density alkali halide layer (CsI), G - accelerating grid.

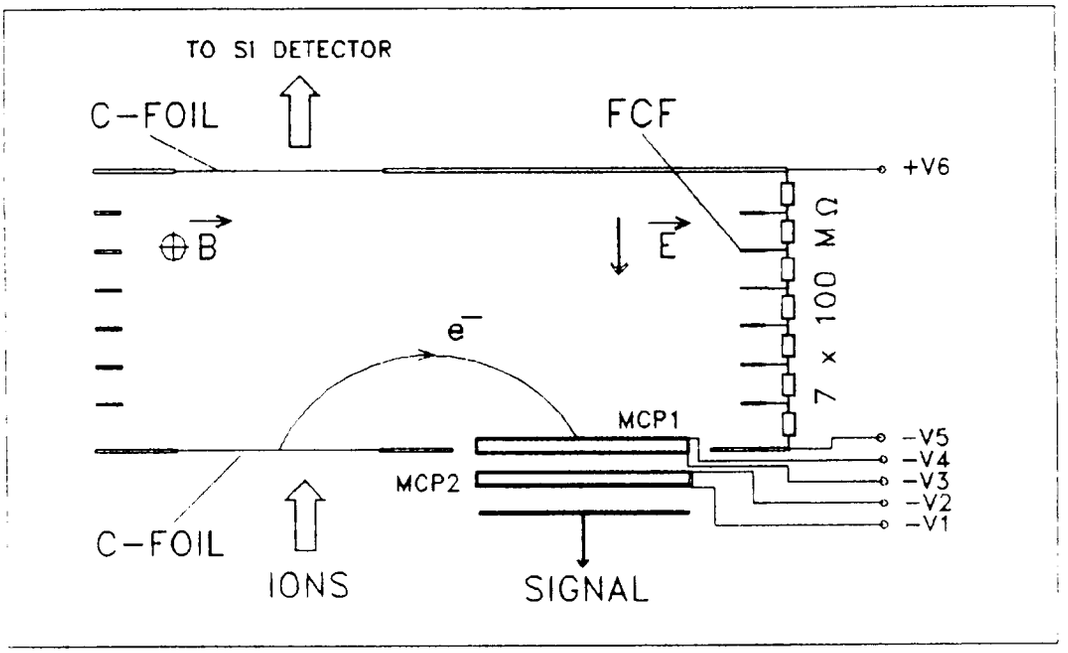

Fig.7. The arrangement of a foil-MCP unit at the SHIP velocity separator.

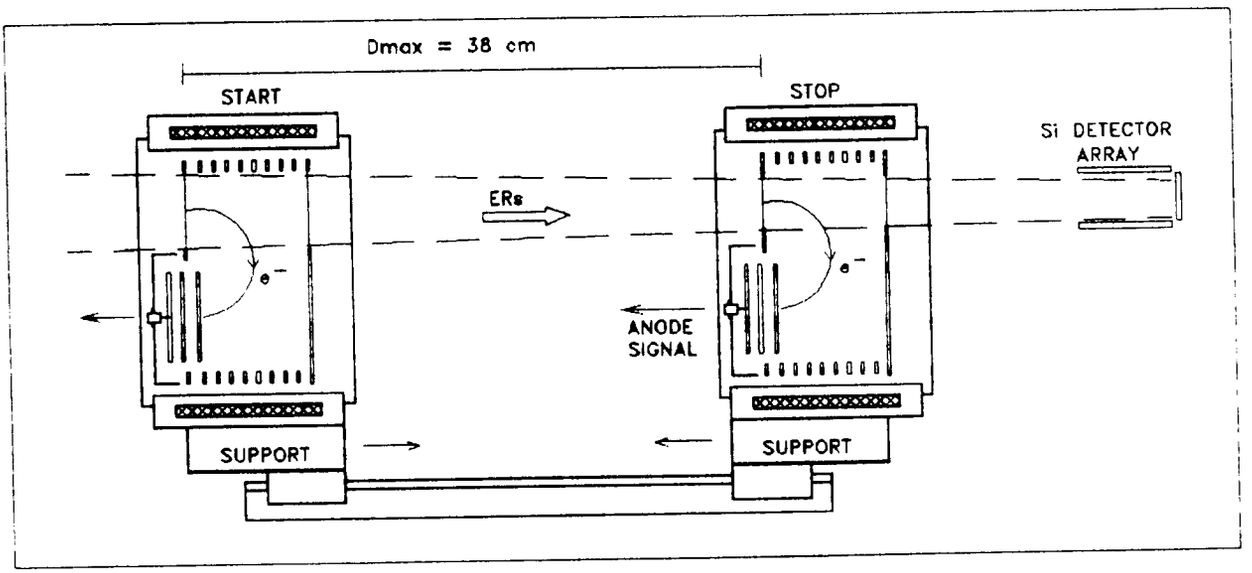

Fig.8. The arrangement of the large area TOF detector system for the SHIP velocity separator. FCF - field correction frames.

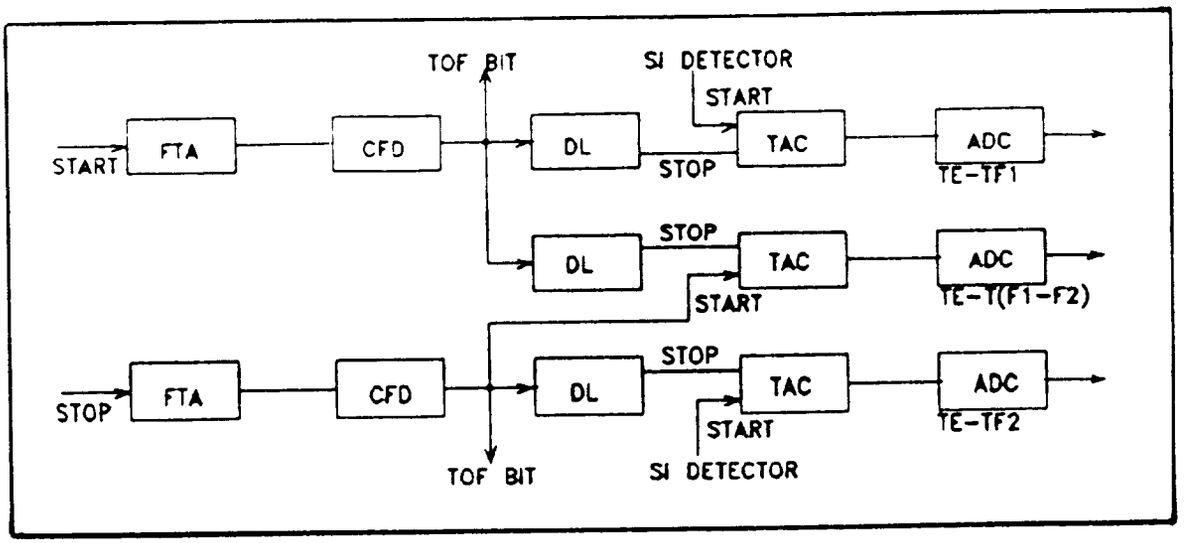

Fig.9. Block-scheme of the electronic setup for the time measurement by the SHIP time-of-flight detector system. FTA - fast timing amplifier, CFD - constant fraction discriminator, DL - delay line, TAC - time-amplitude-convertor, ADC - amplitude-digital-convertor.

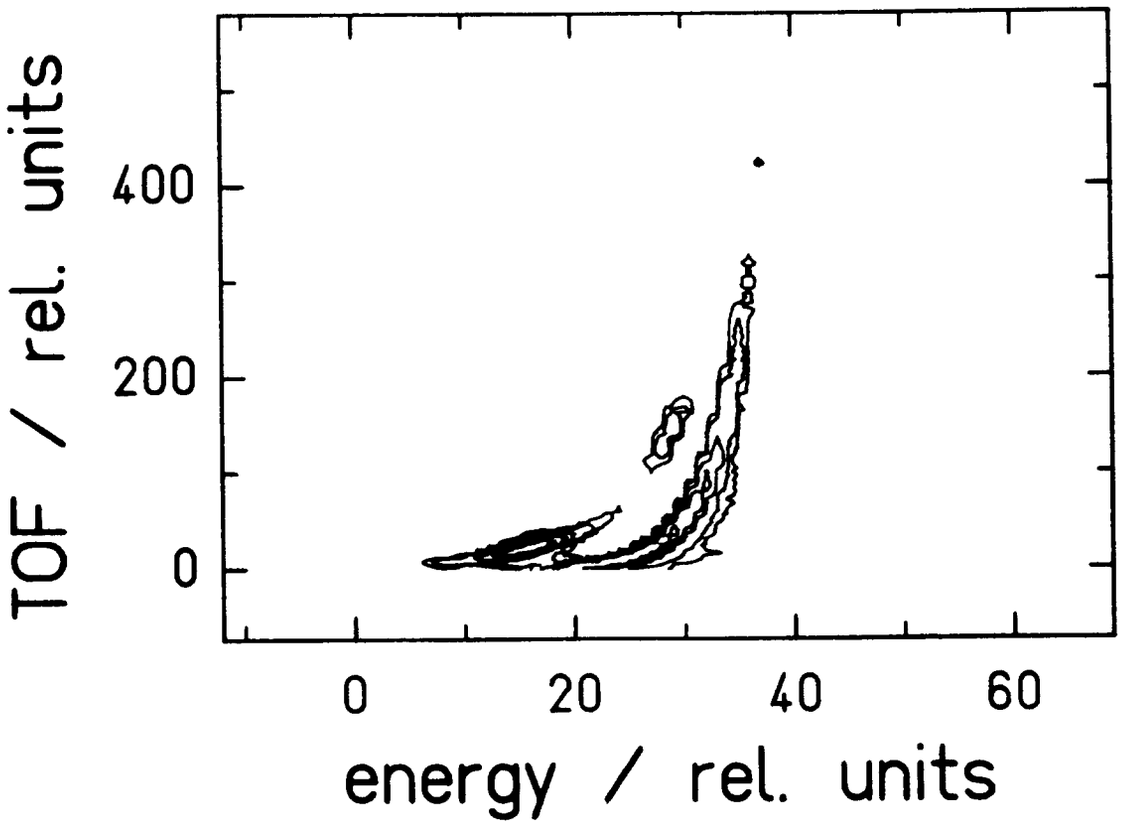

Fig.10. Two-dimensional Time-of-Flight - Energy scatter plot, measured in the reaction of ^{58}Fe + ^{208}Pb at the kinematic separator SHIP.

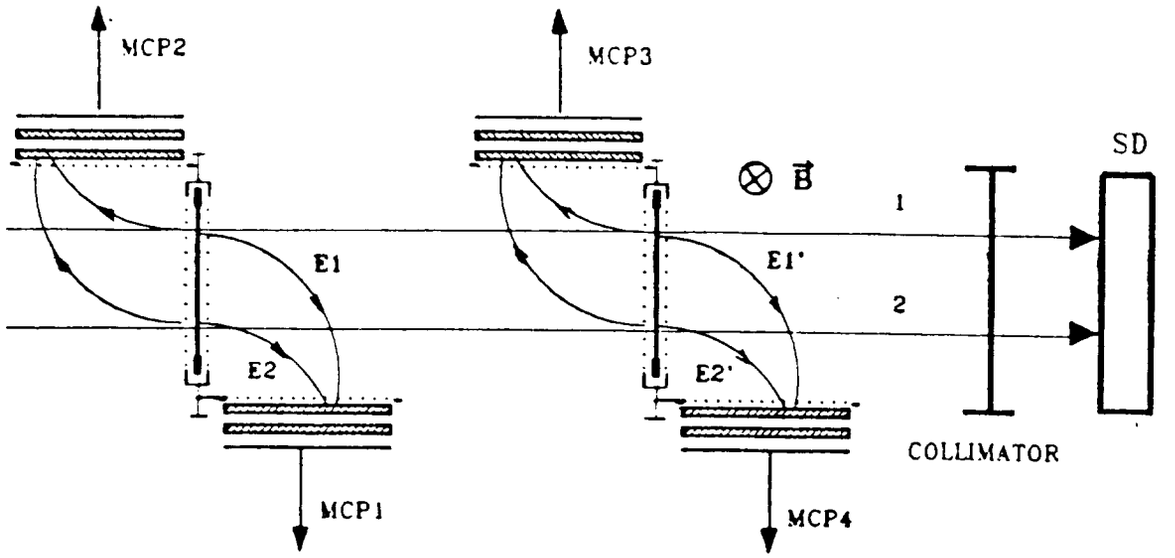

Fig.11. Quarter-turn TOF detectors with accelerating grids, detecting SEs from both sides of the foils. Trajectories from the same side of both foils, for example E1 - E2 and E1'- E2' are identical.

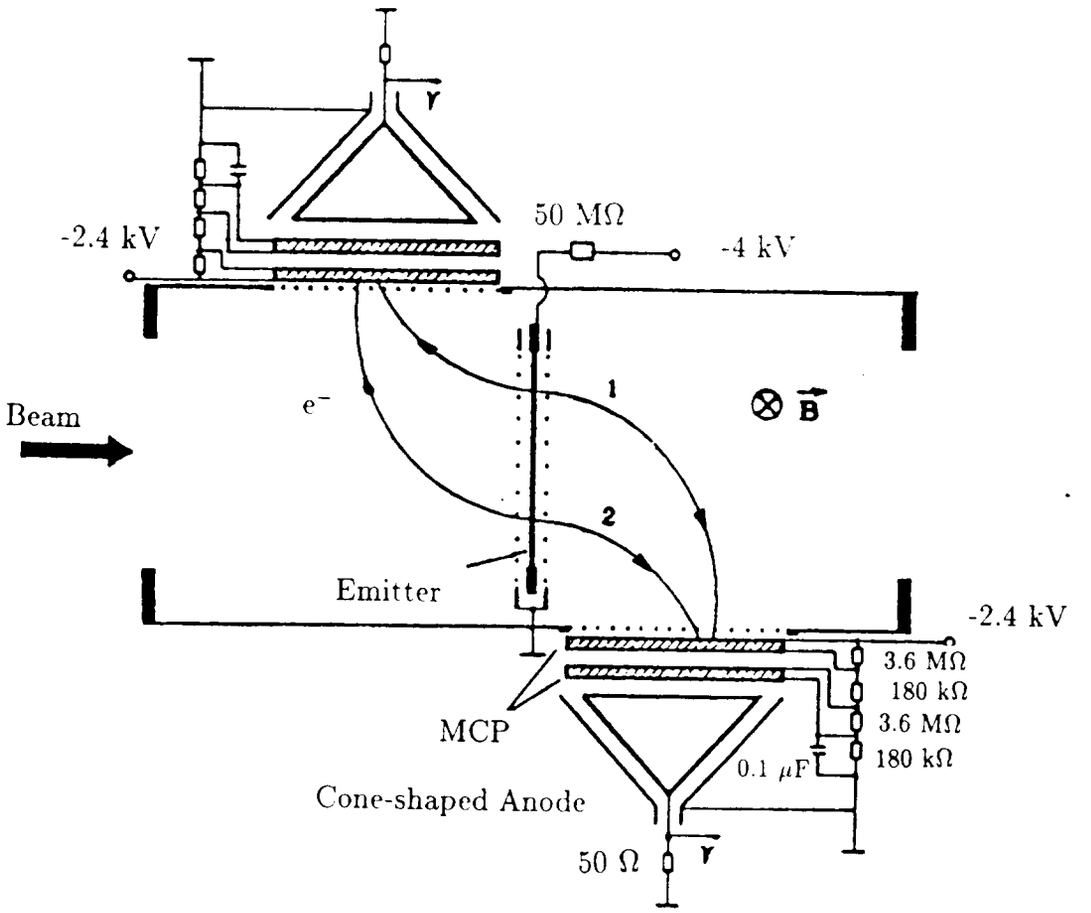

Fig.12. The schematic view of one TOF detector unit, used at the electrostatic separator VASSILISSA

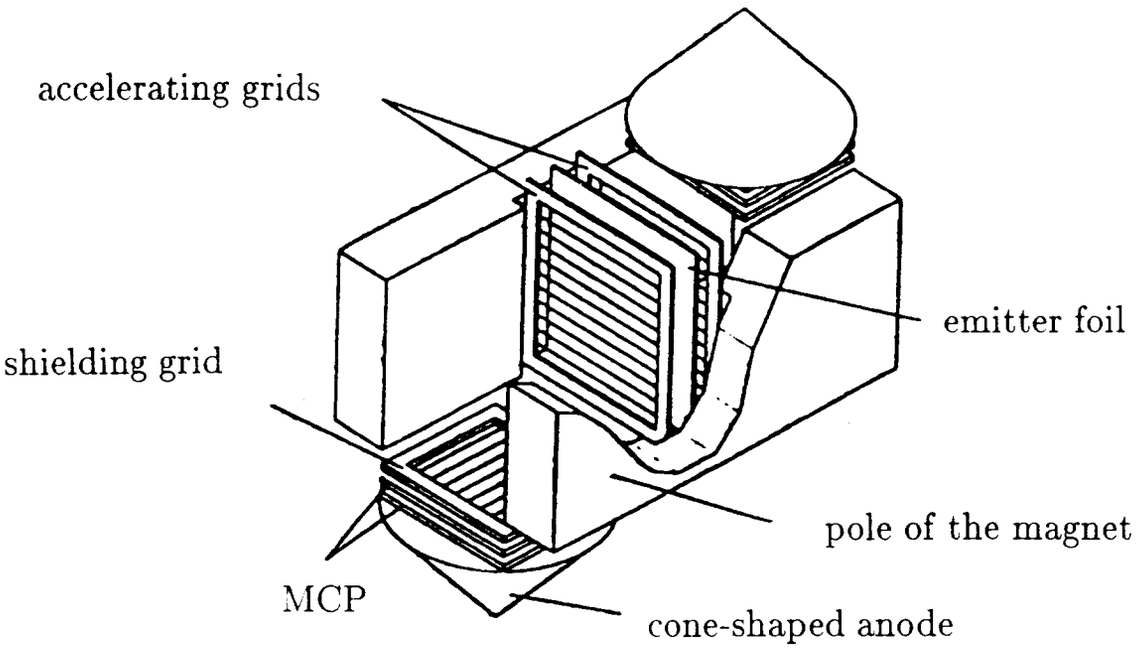

Fig.13. A simplified view of the timing detector. For simplicity the coil, winded on the C-shaped part of the magnet, is not shown.